International Journal of Biological Macromolecules 62 (2013) 225–231

Contents lists available at ScienceDirect

International Journal of Biological Macromolecules

journal homepage: www.elsevier.com/locate/ijbiomac

A nanoporous hydrogel based on vinyl-functionalized alginate for efficient absorption and removal of Pb^{2+} ions

Wenbo Wang, Li Zong, Aiqin Wang*

Center for Eco-material and Green Chemistry, Lanzhou Institute of Chemical Physics, Chinese Academy of Sciences, Lanzhou 730000, PR China

ARTICLE INFO

Article history:
Received 2 August 2012
Received in revised form 23 August 2013
Accepted 23 August 2013
Available online xxx

Keywords:
Vinyl-functionalized alginate
Nanoporous hydrogel
Pb^{2+} absorption
Italic acid

ABSTRACT

Vinyl-functionalized sodium alginate (VSA) was used as matrix and crosslinker to fabricate VSA-*co*-methylacrylic acid-*co*-italic acid (VSA-*co*-MAA-*co*-IA) nano-porous hydrogels using micelle/emulsion as the pore-forming template. ^{1}H NMR, ^{13}C NMR, FTIR and UV–vis analyses proved that vinyl groups were introduced to SA backbone, and the VSA was reacted with the vinyl monomers by a free-radical polymerization to form a hydrogel network. The nano-pores can be uniformly formed in the hydrogels by introducing micelle template as shown by FESEM observations. The absorption properties of the hydrogels for Pb^{2+} ions were investigated by evaluating the absorption isotherm and absorption kinetics. Results showed that the hydrogel has higher absorption capacities for Pb^{2+} ion (432.28 mg/g for 880 mg/L Pb^{2+} solution and 765.75 mg/g for 2800 mg/L Pb^{2+} solution), and the formation of nanoporous structure clearly enhanced the absorption rate by 32.56% (for 880 mg/L Pb^{2+} solution) and 36.79% (for 2800 mg/L Pb^{2+} solution).

1. Introduction

Hydrogels are polymer materials with large amounts of functional groups and particular three-dimensional (3D) network structure, which have been extensively applied in many fields such as water-absorbing materials [1–3], drug-delivery carrier [4,5], nano-reactor [6], antibacterial and tissue engineering materials [7,8], adsorbents [9,10] and carriers of catalysts [11]. Recently, hydrogels were developed as high-efficient adsorbents and used for the absorption and removal of various pollutants (i.e., heavy metals [12–14], dyes [15], ammonium [16], and phenol [17]) from aqueous solution, and satisfactory absorption efficiency can be achieved due to the existence of plentiful functional groups and 3D hydrogel network.

With the growing global concerns on the environmental problem, biopolymers have been intensively concerned as the substitution of petroleum-based raw materials due to their renewable, non-toxic, low-cost, biodegradable and biocompatible advantages [18] and the "green" characteristics [19]. The biopolymers (i.e., chitosan [1,2,20], guar gum [21], starch [22], cellulose [13], and xanthan gum [23]) can form water-insoluble 3D network materials by crosslinking or grafting-crosslinking reaction, and the resultant materials show excellent performance and eco-friendly advantages.

Sodium alginate (SA) is a representative anionic biopolymer composed of α-1,4-L-glucuronic acid (G units) and poly-β-1,4-D-mannuronic acid (M units) in varying proportions by 1–4 linkages. SA can be extracted from marine algae or produced by bacteria, and so it is abundant, renewable, non-toxic, water-soluble, and biodegradable. Generally, SA can be modified through ionic crosslinking, chemical crosslinking and grafting polymerization reaction to derive new material with improved properties [24,25], but the reactivity of raw SA is poor and the additional chemical crosslinkers are required for forming the gel network. Comparatively, the vinyl-functionalization of biopolymer may introduce highly reactive double bonds to its backbone, which allows the graft copolymerization, crosslinking or gelation process more efficiently [26]. The vinyl-functionalization of biopolymer with the modifier glycidyl methacrylate (GMA) through a transesterification and epoxy ring-opening reaction has been considered as a promising strategy to produce vinyl-polysaccharide [27–29]. However, rare research regards on the development of vinyl-functionalized SA and its nano-porous hydrogel up to now.

Based on above background, we introduced vinyl groups onto SA backbone through the modification reaction with GMA for improving its reactive activity and forming a macromolecular crosslinker. The VSA, as a matrix and crosslinker, can easily polymerize with MMA and double-carboxyl IA monomers to form a nano-porous hydrogel (VSA-*co*-MAA-*co*-IA) using the micelle composed of sodium dodecyl sulfonate (SDS) and *n*-Octane (*n*-OT) as the pore-forming template. The structure and morphologies of VSA and the hydrogels were confirmed with ^{1}H NMR, ^{13}C NMR, UV–vis, FTIR

* Corresponding author. Tel.: +86 931 4968118; fax: +86 931 8277088.
E-mail addresses: aqwang@licp.cas.cn, aqwang@lzb.ac.cn (A. Wang).

0141-8130/$ – see front matter © 2013 Elsevier B.V. All rights reserved.
http://dx.doi.org/10.1016/j.ijbiomac.2013.08.038

and FESEM techniques. The absorption properties of the hydrogels for Pb^{2+} ions were systematically evaluated by studying the effect of initial Pb^{2+} concentration and contact time on absorption.

2. Experimental

2.1. Materials

Sodium alginate (SA) with a kinetic viscosity of 20 cp (1.0 wt% aqueous solution) at 20 °C was purchased from Shanghai Chemical Reagents Co. (Shanghai, China). Glycidyl methacrylate (GMA, AR grade) was purchased from ShangHai Daocheng Chemical Co., LTD, Hongkong, China. Methylacrylic acid (MAA, chemically pure) was purchased from Tianjin Kermel Chemical Reagents Development Center (Tianjin, China) and Italic acid (IA, Chemically pure) was purchased from Aladdin Reagent Company. Ammonium persulfate (APS, analytical grade, Xi'an Chemical Reagent Factory, China) was recrystallized before use. *n*-Octane (*n*-OT, AR grade), sodium dodecyl sulfonate (SDS) and lead chloride ($PbCl_2$) was purchased from Tianjin Kermel Chemical Reagents Development Center. All other reagents were of analytical grade and all solutions were prepared using distilled water.

2.2. Preparation of VSA

SA powder (50 g) was dissolved in 3 L of distilled water in a 5 L glass reactor under mechanically stirring to form a homogeneous solution, and then the pH value of the solution was adjusted to 10.5 using 0.5 mol/L NaOH solution. Then, the solution of GMA (100 g) in 50 mL anhydrous ethanol was added dropwise, and the reaction temperature was risen to 60 °C and reacted for 10 h. After this period, modified SA (denoted as VSA) was precipitated in large amount of ethanol, washed with ethanol and separated by suction filtration. The resultant solid was re-dissolved in distilled water, and precipitated in ethanol. The same dissolution–precipitation process was conducted for 3 times to remove the residual GMA. Finally, the precipitate was lyophilized for 12 h to obtain VSA sample.

2.3. Determination of substitution degree (SD)

Typically, GMA was dissolved in water/methanol (4/1, v/v) mixture solvents to form a sets of solutions (0.02, 0.039, 0.078, 0.156 and 0.313 mol/L) used to establish the standard curve. The absorbance of each solution was determined with UV spectroscopy at the maximum absorbance wavelength of 215 nm. The resultant standard curve follows the equation: $A = 0.0017 + 8.2972c$ ($R = 0.9999$; c is the concentration of GMA (mol/L), and A is the absorbance at 215 nm). The 50 mg VSA sample was dissolved in 100 mL water/methanol (4/1, v/v) mixture solvents, and the absorbance of the solution was determined by UV spectroscopy at 215 nm. The substitution degree (SD) of vinyl groups on VSA can be calculated by the slope of above straight lines, and the SD value is 0.37 mmol/g (denoted as the molar amount of the vinyl groups existed in per gram of VSA).

2.4. Synthesis of VSA-co-MAA-co-IA nano-porous hydrogels

15 mg SDS was dissolved in 20 mL distilled water in a 50 mL two-neck flask, and then 0.25 mL *n*-OT was added under continuous magnetic stirring. 1 h later, 0.5 g VSA was added and fully dissolved in the solution. Then, the mixture solution containing 3.76 g MAA, 0.24 g IA, 30 mg APS, 5 mL water and certain amount of NaOH was slowly added to the reaction flask and continuously stirred for 4 h to form a homogeneous solution. The reaction flask was purged with N_2 for 30 min and then placed in an oil bath (70 °C) under continuous stirring. After reacted for 3 h, the flask was cooled to room temperature and the gel product was fully washed with distilled water. Finally, the product was repeatedly soaked in acetone to dewater, and refuxed in hot ethanol for 12 h to remove the surfactant SDS and *n*-OT (repeated for 3 times). The resultant xerogel was ground and passed through a 40–80 mesh sieve (180–380 μm) for use.

2.5. Batch absorption experiments

50 mg of the dry granular sample (180–380 μm) was contacted with 25 mL aqueous solutions of $PbCl_2$ (880 and 2800 mg/L, pH 5.0), and the mixture was agitated in a thermostatic shaker (THZ-98A) at 30 °C and 120 rpm for 60 min to achieve absorption equilibrium. The adsorbents were separated by a sintered glass filter and the Pb^{2+} concentration in the filtrate was determined by atomic absorption spectrophotometer (AAS, Hitachi Z-8000). The absorption capacities of the hydrogel for Pb^{2+} can be calculated by Eq. (1):

$$q = \frac{0.025C_o - V_eC_e}{w} \quad (1)$$

where q is the absorption amount of the hydrogel on Pb^{2+} ion at time t (q_t, mg/g) or at equilibrium (q_e, mg/g), C_o and C_e are the initial and final concentration of ions (mg/L), V_e is the liquid-phase volume of the Pb^{2+} solution after absorption (L), and w is the mass of the sample used (g). In this work, a set of Pb^{2+} solutions with the concentrations of 400–3200 mg/L were used to study the absorption isotherms.

The absorption kinetics was evaluated as the following procedure: 50 mg xerogel particles (SA3 and SA10) were soaked in the aqueous solutions of 880 and 2800 mg/L Pb^{2+} ions under agitating. The solution was then separated from the adsorbent by filtering at certain intervals (0–3600 s). The absorption capacities (q_t, mg/g) at a given moment t were calculated using Eq. (1).

2.6. Characterizations

FTIR spectra were recorded on a Nicolet NEXUS FTIR spectrometer in 4000–400 cm^{-1} region using KBr pellets. ^1H NMR and ^{13}C NMR analyses were conducted in Bruker AVANCE III 600 MHz nuclear magnetic resonance chemical analyzer (Germany). The Dimethyl sulfoxide-d6 (DMSO-d6) solution of GMA, the D_2O solutions of SA and VSA were prepared in NMR tubes of 5 mm diameter and used to collect the NMR spectra using tetramethylsilane (TMS) as the reference line. The chemical shift was reported as δ values (ppm). UV–vis analysis was performed on a UV-vis spectrophotometer (SPECORD 200, Analytik Jera AG), and the sample was dissolved in methanol/water mixture solvent (1:4, v/v). The surface morphologies of the samples were examined using a JSM-6701F Field Emission Scanning Electron Microscope (JEOL) after coating the sample with gold film.

3. Results and discussion

3.1. Preparation of VSA-co-MAA-co-IA nano-porous hydrogels

The VSA-*co*-MMA-*co*-IA hydrogels with 3D network structure can be formed by a typical radical polymerization and crosslinking reaction (Fig. 1). The vinyl groups were introduced onto SA by its reaction with GMA. Under heating, the initiator APS can be decomposed by homolytic cleavage to generate sulfate anion-radicals [30]. These radicals may simultaneously trigger the double bonds on VSA chain and adjacent monomers (MAA and IA) to process a rapid polymerization and chain propagation. These polymer chains formed by MAA and IA may connect two or more SA chains

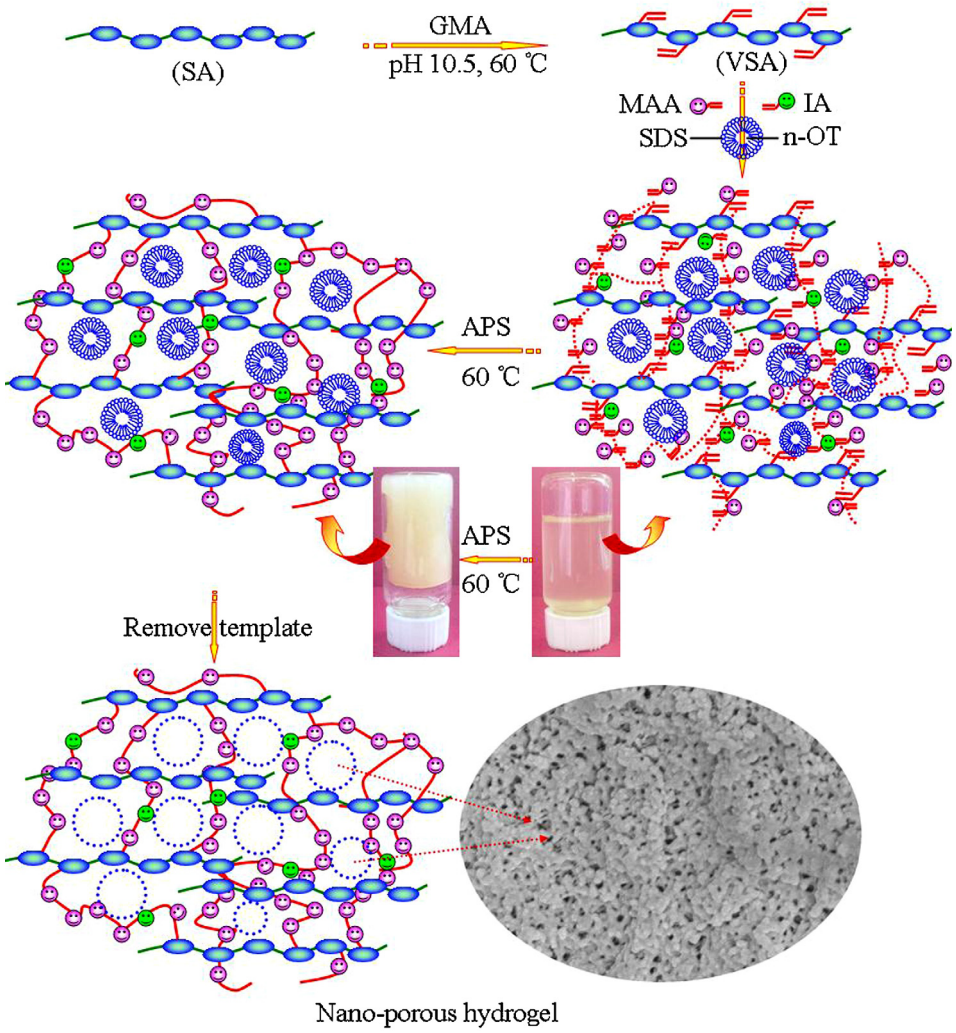

Fig. 1. The in situ formation mechanism of the nano-porous three-dimensional network hydrogel.

to form a crosslinked network structure. In this process, VSA acts as a matrix and sugar crosslinker. In the process of polymerization, the SDS and *n*-OT may form uniformly distributed emulsion micelle in the reactants, which may be fixed in the hydrogel after crosslinking. After removing the emulsion micelle, numerous nano-pores can be formed in the hydrogel (Fig. 1).

3.2. ^{1}H NMR and ^{13}C NMR spectroscopies

The ^{1}H NMR and ^{13}C NMR spectra of GMA, SA and VSA were collected for confirming the formation of VSA (Fig. 2a and b). The ^{1}H NMR spectrum of SA shows the characteristic of non-anomeric (δ 3.55–4.01) and anomeric protons (δ 4.86). Compared with the spectrum of SA, the new resonance peaks at δ 1.80 ppm (methyl protons), δ 5.60 and 6.02 ppm (two protons of the double bond in the methacryloyl groups) appeared in the resonance spectrum of VSA. The ^{1}H NMR and ^{13}C NMR spectrogram of VSA is similar with that of GMA-modified cashew gum [26], indicating that the modification mechanism of SA and cashew gum with GMA is similar. The ^{13}C NMR spectrum of SA shows the sugar carbons in the range of δ 63.5–102.18 ppm. After forming VSA, the new peaks at δ 19.46 ppm (methyl carbon), δ 129.28 and 138.31 ppm (vinyl carbons) and δ 171.86 ppm (carbonyl carbon) appeared. These results confirmed that SA was successfully modified with GMA and vinyl groups were introduced onto SA backbone.

The modification mechanism of polymer with GMA was systematically and intensively studied by previous works [26–29,31]. The resonance peaks of glyceryl and the ^{1}H NMR peaks at δ 5.60 and 6.02 ppm (H atom on vinyl carbon) was clearly observed. It was concluded that the reaction mechanism of SA with GMA are mainly involved with the ring-opening mechanism [31].

3.3. FTIR and UV–vis spectra

As shown in Fig. 3, SA shows the characteristic absorption bands at 1097 cm^{-1} and 1031 cm^{-1} (stretching vibration of C—OH groups), at 1616 cm^{-1} (asymmetrical stretching vibration of —COO^{-} groups), 1418 cm^{-1} (symmetrical stretching vibration of —COO^{-} groups). After modified with GMA, the new bands at 1711 cm^{-1} (the stretching vibration of —C=O of conjugated ester groups) appeared, and the C—O stretching vibration peak at 1175 cm^{-1} was obviously enhanced, indicating that SA was successfully modified with GMA [26,27]. In order to confirm the existence of vinyl groups (C=C—H), the UV spectra of GMA, SA, VSA and the hydrogels were determined (Fig. 4). The SA has no absorbance in the scanning wavelength range (200–500 nm), and GMA shows a stronger absorbance of vinyl groups at 215 nm. After modified SA with GMA, the UV spectra also show an absorbance peak at 215 nm, which can confirm the vinyl groups were successfully introduced onto SA.

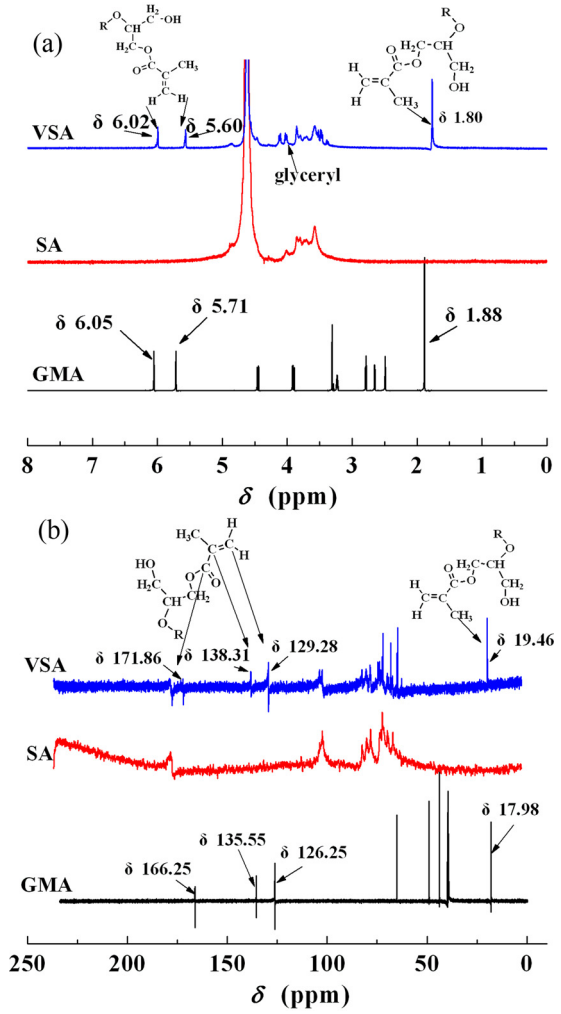

Fig. 2. (a) ^{1}H NMR spectrum of GMA (in DMSO-d6), SA (in D_2O) and VSA (in D_2O); (b) ^{13}C NMR spectra of GMA (in DMSO-d6), SA (in D_2O) and VSA (in D_2O).

After forming hydrogel, the new absorption bands at 1667 cm^{-1} (asymmetrical stretching vibration of —COOH groups) and 1556 cm^{-1} (asymmetrical stretching vibration of $—COO^-$ groups) were observed, indicating the MAA and IA monomers were

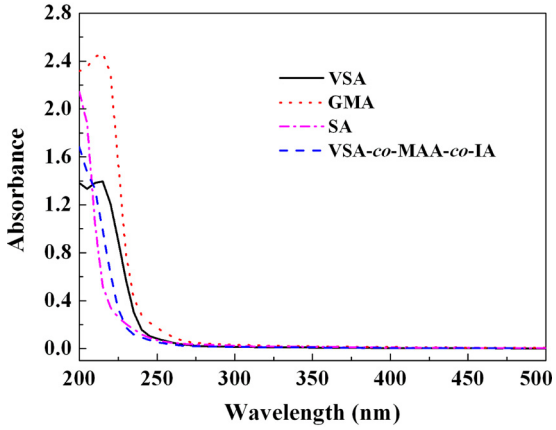

Fig. 4. UV–vis spectra of SA, GMA, VSA and VSA-*co*-MAA-*co*-IA nano-porous hydrogel (S3).

polymerized with VSA. No absorption peak can be observed in the UV–vis spectra of the hydrogel, indicating that the vinyl groups of VSA were reacted with the monomers.

3.4. FESEM analysis

As depicted in Fig. 5, the VSA-*co*-MAA-*co*-IA hydrogel prepared without adding pore-forming agent (SA10) shows a dense and smooth surface, and no pores were observed (Fig. 5a). However, after adding the emulsion template composed of SDS and *n*-OT, the formed hydrogels exhibit uniform porous structure with the pore diameter of about 20–60 nm (Fig. 5b–d). This indicates the emulsion micelle formed by SDS and *n*-OT may act as an effective pore-forming template and induce the generation of nano-pores. The formation of pores in hydrogel may reduce the mass-transfer resistance, and facilitate to the diffusion of the adsorbate into the interior gel network.

3.5. Feed composition and absorption properties

Table 1 gives the feeding composition, absorption capacity (AC) and removal rate (RR) of each hydrogel. As is shown, the absorption capacity and removal rate of the hydrogel increased with increasing the dosage of IA and neutralization degree (ND), until the optimal absorption capacity (432.28 mg/g) and removal rate (98.25%)

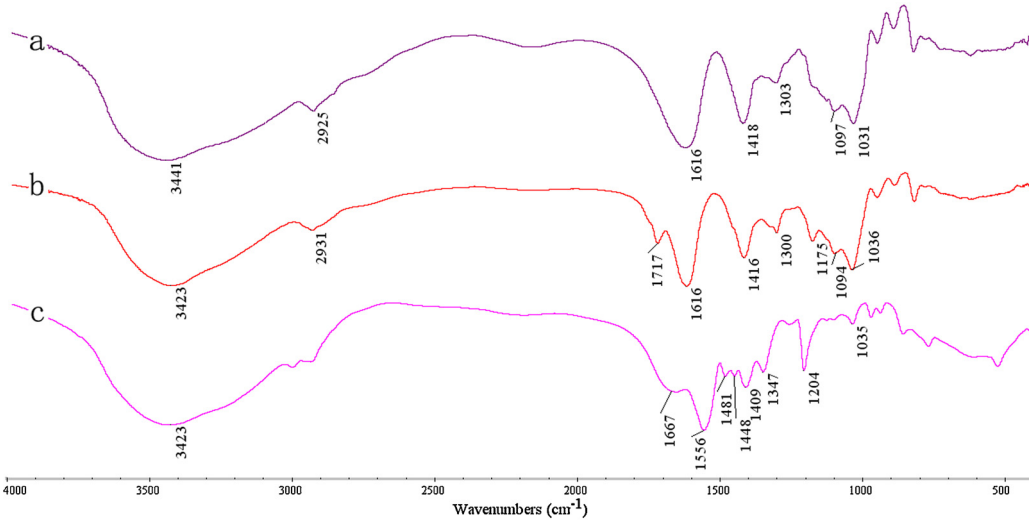

Fig. 3. FTIR spectra of SA, VSA and VSA-*co*-MAA-*co*-IA nano-porous hydrogel (SA3).

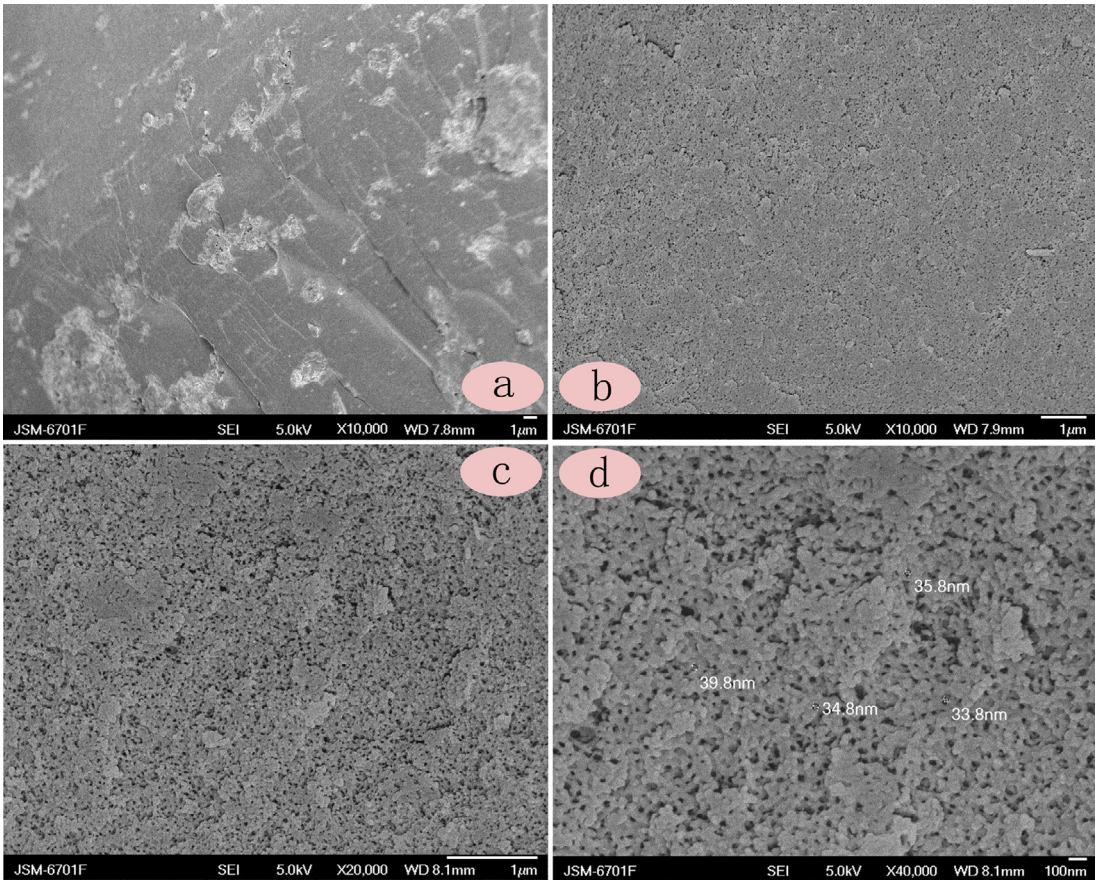

Fig. 5. FESEM micrographs of (a) non-porous hydrogel SA10, and (b–d) the VSA-*co*-MAA-*co*-IA hydrogel (S3) at different magnifications.

Table 1
The feeding composition of the hydrogels and the absorption properties for Pb^{2+} ion (initial Pb^{2+} concentration, 880 mg/L).

Sample	VSA (g)	MAA (mmol)	IA (mmol)	ND (%)	SDS (mg)	*n*-OT (mL)	AC (mg/g)	RR (%)
SAH0	0.5	46.50	0.00	80	15	0.25	387.61	88.09
SAH1	0.5	45.87	0.63	80	15	0.25	399.52	90.80
SAH2	0.5	45.25	1.25	80	15	0.25	414.50	94.21
SAH3	0.5	44.63	1.87	80	15	0.25	432.28	98.25
SAH4	0.5	43.37	3.13	80	15	0.25	420.47	95.56
SAH5	0.3	44.63	1.87	80	15	0.25	413.93	94.08
SAH6	0.7	44.63	1.87	80	15	0.25	426.64	96.96
SAH7	0.9	44.63	1.87	80	15	0.25	421.85	95.88
SAH8	0.5	44.63	1.87	70	15	0.25	406.23	92.33
SAH9	0.5	44.63	1.87	90	15	0.25	415.41	94.41
SAH10	0.5	44.63	1.87	80	0	0	424.43	96.69

was achieved at the MAA/IA molar ratio of 23.87 and the ND of 80%. This is because that, (i) IA is a double carboxylic monomer, and so its introduction may increase the total amount of carboxylate groups in the hydrogel. As a result, the absorption site used to chelating Pb^{2+} ion was increased and the absorption capacity was improved; (ii) with increasing the ND to 80%, more —COOH groups were transferred into —COO^- groups. The —COO^- groups have relatively stronger complexing ability to Pb^{2+} ion, and so the absorption capacity of the hydrogel to Pb^{2+} ion was increased [31].

3.6. *Effect of initial Pb^{2+} concentrations on absorption*

As shown in Fig. 6, the absorption capacity of the hydrogels sharply increased with increasing the initial Pb^{2+} concentration as a result of increasing the absorption driving force, until the absorption equilibrium was almost reached at the initial concentration of 2800 mg/L. In order to illustrate the absorption process and

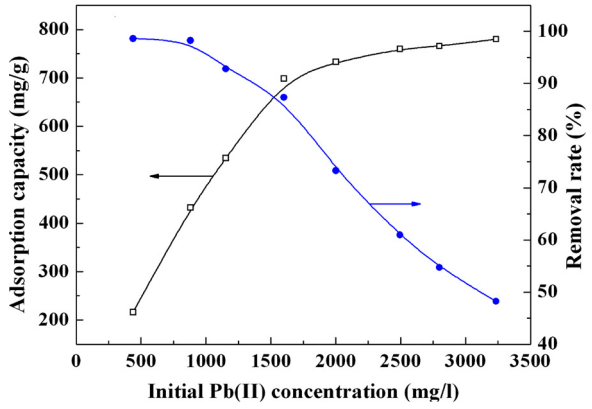

Fig. 6. Effect of initial Pb^{2+} concentration on adsorption capacities and removal rate.

Table 2
Fitted parameters for the absorption for Pb^{2+} ion.

Langmuir model			
q_m (mg/g)	b (L/mg)	R_L	R^2
787.40	0.0378	0.00811~0.05696	0.9999
Freundlich model			
k	n		R^2
204.17	5.0896		0.9249
Dubinin–Radusckevich model			
q_m (mg/g)	β (mol/kJ)^2	E (kJ/mol)	R^2
1157.01	0.0021	15.4303	0.9512

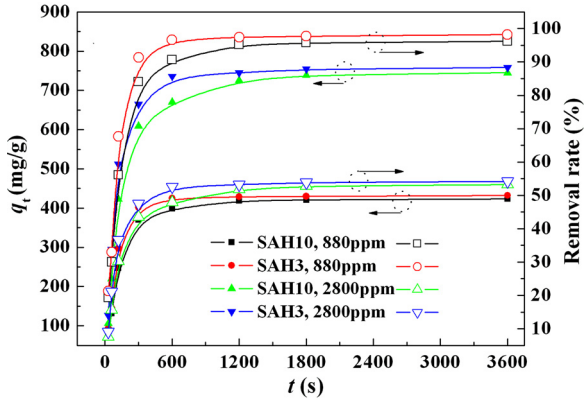

Fig. 7. Adsorption kinetic curves of the hydrogels with porous (SAH3) and without pores (SAH10) at the initial Pb^{2+} concentration of 880 mg/L and 2800 mg/L.

mechanism, three most common isotherm equations including Langmuir (Eq. (2)) [32], Freundlich (Eq. (4)) [33] and Dubinin–Radushkevich (D-R) (Eq. (5)) [34] models were employed.

$$\frac{C_e}{q_e} = \frac{1}{q_m b} + \frac{C_e}{q_m} \tag{2}$$

$$R_L = \frac{1}{1 + bC_i} \tag{3}$$

Here, q_e is the equilibrium absorption capacities of the hydrogels for Pb^{2+} ions (mg/g), C_e is the concentration of residual Pb^{2+} ions in the solution after absorption (mg/L), q_m is the maximum absorption capacity of the adsorbent (mg/g), and b is the Langmuir absorption constant (L/mg) and is related to the free energy of adsorption. C_i is the initial concentration of Pb^{2+} ions.

The essential feature of the Langmuir isotherm is R_L. It is a dimensionless separation factor or equilibrium parameter, and its value can reflect the favorable or unfavorable absorption isotherm [35]. The R_L value between 0 and 1 indicates favorable absorption, $R_L > 1$ suggests unfavorable absorption and $R_L = 1$ reveals linear absorption process.

The Freundilich model is expressed as follows:

$$\log q_e = \log\ k + \left(\frac{1}{n}\right) \log C_e \tag{4}$$

Here, k (L/g) and n (dimensionless) are the Freundlich isotherm constant and the heterogeneity factor, respectively.

The D-R model is expressed as follows:

$$\ln q_e = \ln q_m - \beta\varepsilon_2 \tag{5}$$

$$E = (2\beta)^{-0.5} \tag{6}$$

Here, β is the constant related to the mean free energy of absorption (mol/kJ)^2 and ε is the Polanyi potential (kJ/mol). The parameter ε is the amount of energy required to pull a sorbed molecule from its absorption site to infinity [36] and is equal to $RT\ln(1 + (1/C_e))$. R (=8.314 J/(mol K)) is the gas constant and T (K) is the absolute temperature.

Table 2 shows the absorption parameters obtained by fitting the experimental absorption data with the Langmuir (plotting C_e/q_e vs. C_e), Freundlich (plotting $\log q_e$ vs. $\log C_e$) and D-R (plotting $\ln q_e$ vs. ε^2) models. The obtained linear correlation coefficients $R^2 = 0.9249$ for Freundlich isotherm, $R^2 = 0.9512$ for D-R model, but can reach $R^2 = 0.9999$ for Langmuir isotherm model. The theoretical maximum absorption capacity (787.4 mg/g) fitted by Langmuir isotherm is more close to the experimental value, indicating that the Langmuir isotherm model is suitable for describing the absorption isotherm. Thus, by analyzing the fitting result, the absorption of the hydrogel for Pb^{2+} tends to be a monolayer absorption mechanism, and the absorption sites are energetically equivalent [32].

It can be noticed from Table 2, the R_L value is smaller than 1. This indicates that the absorption of the hydrogel for Pb^{2+} ion is a favorable process.

As shown in Table 2, the calculated E value is 15.4303 kJ/mol, which is larger than 8 kJ/mol corresponding to a physical adsorption [37]. This indicates that the absorption of the hydrogel for Pb^{2+} ion is a chemical absorption process that is different from the physical adsorption. In this process, when the hydrogel was contact with the solution containing Pb^{2+} ion, the Pb^{2+} ions may transport to the hydrogel due to the electrostatic attraction between the $-COO^-$ groups and Pb^{2+} ions, and then some Pb^{2+} ions entered the gel network. When the Pb^{2+} ion was contact with $-COO^-$ groups, the complexing interaction occurred and the Pb^{2+} ion was fixed in the hydrogel. During the absorption, the hydrogel may be slightly swollen, and the 3D gel network may expand to accelerate the transport of Pb^{2+} ions.

3.7. Absorption kinetics

As shown in Fig. 7, the amount of Pb^{2+} ion adsorbed by the hydrogels was rapidly increased with prolonging the absorption time (t, s), and the equilibrium almost reached within 5 min. The dynamic absorption mechanism such as mass transfer and chemical reaction can be explored by fitting the experimental data with the pseudo first-order (Eq. (7)) and pseudo-second-order (Eq. (8)) kinetic models as shown follows [38].

$$\log(q_e - q_t) = \log\ q_e - \left(\frac{k_1}{2.303}\right) t \tag{7}$$

$$\frac{t}{q_t} = \frac{1}{k_2 q_e^2} + \frac{t}{q_e} \tag{8}$$

where q_e and q_t are the absorption capacities of the hydrogel for Pb^{2+} ion (mg/g) at equilibrium state and time t (s), respectively. The absorption rate constants for pseudo-first-order (k_1, s^{-1}) and pseudo-second-order (k_2, mg/(g s)) kinetics can be obtained by the slope and intercept of the straight lines $\log(q_e - q_t)$ versus t and t/q_t versus t, respectively. The initial absorption rate constant k_{2i} (mg/(g s)) for pseudo-second-order absorption kinetic model can be calculated using the relation $k_{2i} = k_2 q_e^2$ (Table 3).

The absorption kinetic parameters were obtained by fitting the experimental data with pseudo-first-order and pseudo-second-order kinetic model and the results were shown in Table 3. As can be seen, the theoretical q_e value for pseudo-first-order kinetic model has obvious deviation with the experimental value, and

Table 3
Estimated absorption kinetic parameters for Pb^{2+} ion.

Samples	Pseudo-first-order model				Pseudo-second-order model			
	$q_{e,exp}$ (mg/g)	$q_{e,cal}$ (mg/g)	K_1 (s^{-1})	R^2	$q_{e,cal}$ (mg/g)	k_2 ($\times 10^5$ g/(mg s))	k_{2i} (mg/(g s))	R^2
Initial Pb^{2+} concentration, 880 mg/L								
SAH10	424.43	226.45	0.00283	0.9671	433.51	2.6539	4.9875	0.9997
SAH3	432.28	157.89	0.00288	0.9049	440.48	3.4076	6.6116	0.9998
Initial Pb^{2+} concentration, 2800 mg/L								
SAH10	745.05	464.41	0.00256	0.9741	753.19	1.1626	6.5954	0.9996
SAH3	758.21	341.85	0.00272	0.9472	769.26	1.5245	9.0211	0.9995

the correlation coefficients (R^2) is lower (<0.9741) for each sample at each initial Pb^{2+} concentration. However, the q_e value calculated by pseudo-second-order kinetic model is close to the experimental value, and the R^2 value is also higher (>0.9998). This indicates that the dynamic absorption behavior of the hydrogel for Pb^{2+} ion obeys pseudo-second-order kinetic model. And the absorption process of the hydrogel for Pb^{2+} ion is probably controlled by the chemical absorption mechanism [39,40]. The higher initial concentration is favorable to the fast absorption in contrast to lower concentration due to the greater absorption driving force generated by higher Pb^{2+} concentration. For each hydrogel, the initial absorption rate constants follow the order of SAH3 (9.0211 mg/(g s) for 2800 mg/L) > SAH3 (6.6116 mg/(g s) for 880 mg/L) > SAH10 (6.5954 mg/(g s) for 2800 mg/L) > SAH10 (4.9875 mg/(g s) for 880 mg/L), indicating that the formation of nano-pores in the hydrogel is favorable to improve the absorption rate for Pb^{2+} ions at different initial concentration.

4. Conclusion

The biopolymer SA was modified with GMA to derive vinyl-functionalized SA (VSA), and VSA was used as "macro-monomer" and crosslinker to prepare SA-*co*-MAA-*co*-IA hydrogels with excellent Pb^{2+} absorption properties. The emulsion/micelle composed of SDS and *n*-OT was introduced during polymerization process to create a nano-porous structure. The structure of VSA and the hydrogels was confirmed by ^1H NMR, ^{13}C NMR, FTIR and UV spectra, and the pores with the size of 20–60 nm was observed by FESEM technology. The hydrogels show satisfactory absorption properties for Pb^{2+} ion, and the optimal hydrogel was obtained at the recipe of VSA, 0.5 g; MAA, 44.63 mmol; IA, 1.87 mmol; neutralization degree, 80%; SDS, 15 mg; *n*-OT, 0.25 mL. The equilibrium absorption isotherm was well fitted by the Langmuir isotherm in its linear form, and the absorption kinetics follow the quasi-second order kinetic model, which suggests a chemical absorption process related to the functional groups. The formation of nano-porous structure can clearly enhanced the initial absorption rate constant from 4.9875 to 6.6116 mg/(g s) (initial Pb^{2+} concentration, 880 mg/L), from 6.5954 to 9.0211 mg/(g s) (initial Pb^{2+} concentration, 2800 mg/L). The biopolymer-based nano-porous hydrogel with excellent absorption properties and eco-friendly advantages can be developed as a potential heavy metal adsorbent for the substitution of traditional adsorbents.

Acknowledgments

This work is supported by the National Natural Science Foundation of China (No. 20877077) and "863" Project of the Ministry of Science and Technology, PR China (No. 2013AA031403).

References

[1] A. Zamani, D. Henriksson, M.J. Taherzadeh, Carbohydr. Polym. 80 (2010) 1091–1101.
[2] C. Spagnol, F.H.A. Rodrigues, A.G.B. Pereira, A.R. Fajardo, A.F. Rubira, E.C. Muniz, Carbohydr. Polym. 87 (2012) 2038–2045.
[3] W.B. Wang, A.Q. Wang, Carbohydr. Polym. 82 (2010) 83–91.
[4] N. Bhattarai, J. Gunn, M.Q. Zhang, Adv. Drug Delivery Rev. 62 (2010) 83–99.
[5] A. Giri, M. Bhowmick, S. Pal, A. Bandyopadhyay, Int. J. Biol. Macromol. 49 (2011) 885–893.
[6] P.S. Gils, D. Ray, P.K. Sahoo, Int. J. Biol. Macromol. 46 (2010) 237–244.
[7] S.V. Vlierberghe, P. Dubruel, E. Schacht, Biomacromolecules 12 (2011) 1387–1408.
[8] S. Nair, N.S. Remya, S. Remya, P.D. Nair, Carbohydr. Polym. 85 (2011) 838–844.
[9] M.M. Bekheit, N. Nawar, A.W. Addison, D.A. Abdel-Latif, M. Monier, Int. J. Biol. Macromol. 48 (2011) 558–565.
[10] N.G. Kandile, A.S. Nasr, Carbohydr. Polym. 85 (2011) 120–128.
[11] B. Léger, S. Menuel, A. Ponchel, F. Hapiot, E. Monflier, Adv. Synth. Catal. 354 (2012) 1269–1272.
[12] J.P. Zhang, A.Q. Wang, J. Chem. Eng. Data 55 (2010) 2379–2384.
[13] Y. Liu, W.B. Wang, A.Q. Wang, Desalination 259 (2010) 258–264.
[14] E.S. Abdel-Halim, S.S. Al-Deya, Carbohydr. Polym. 86 (2011) 1306–1312.
[15] B. Özkahraman, I. Acar, S. Emik, Polym. Bull. 66 (2011) 551–570.
[16] Y.A. Zheng, J.P. Zhang, A.Q. Wang, Chem. Eng. J. 155 (2009) 215–222.
[17] G.F. Pan, K.I. Kurumada, Chem. Eng. J. 138 (2008) 194–199.
[18] I. Šimkovic, Carbohydr. Polym. 74 (2008) 759–762.
[19] S.S. Ray, M. Bousmina, Prog. Mater. Sci. 50 (2005) 962–1079.
[20] N.G. Kandile, A.S. Nasr, Carbohydr. Polym. 78 (2009) 753–759.
[21] W.B. Wang, Y.R. Kang, A.Q. Wang, Sci. Technol. Adv. Mater. 11 (2010) 025006, 10pp.
[22] W. Zou, L. Yu, X.X. Liu, L. Chen, X.Q. Zhang, D.L. Qiao, R. Zhang, Carbohydr. Polym. 87 (2012) 1583–1588.
[23] H. Izawa, J. Kadokawa, J. Mater. Chem. 20 (2010) 5235–5241.
[24] M. Yadav, D.K. Mishra, A. Sand, K. Behari, Carbohydr. Polym. 84 (2011) 83–89.
[25] M. Yadav, K.Y. Rhee, Carbohydr. Polym. 90 (2012) 165–173.
[26] M.R. Guilherme, A.V. Reis, S.H. Takahashi, A.F. Rubira, J.P.A. Feitosa, E.C. Muniz, Carbohydr. Polym. 61 (2005) 464–471.
[27] M.R. Guilherme, T.A. Moia, A.V. Reis, A.T. Paulino, A.F. Rubira, L.H.C. Mattoso, E.C. Muniz, E.B. Tambourgi, Biomacromolecules 10 (2009) 190–196.
[28] A.V. Reis, M.R. Guilherme, O.A. Cavalcanti, A.F. Rubira, E.C. Muniz, Polymer 47 (2006) 2023–2029.
[29] M.R. Guiherme, A.R. Fajardo, T.A. Moia, M.H. Kunita, M.C. Gonçalves, A.F. Rubira, E.B. Tambourgi, Eur. Polym. J. 46 (2010) 1465–1474.
[30] F.L. Buchholz, T. Graham, Modern Superabsorbent Polymer Technology, Wiley-VCH, New York, 1998.
[31] (a) A.V. Reis, A.R. Fajardo, I.T.A. Schuquel, M.R. Guilherme, G.J. Vidotti, A.F. Rubira, E.C. Muniz, J. Org. Chem. 74 (2009) 3750–3757;
(b) Y.A. Zheng, D.J. Huang, A.Q. Wang, Anal. Chim. Acta 687 (2011) 193–200.
[32] I. Langmuir, J. Am. Chem. Soc. 40 (1918) 1361–1403.
[33] H.M.F. Freundlich, Z. Phys. Chem. 57 (1906) 385–470.
[34] M.M. Dubinin, L.V. Radushkevich, Proc. Acad. Sci. Phys. Chem. Sect. U.S.S.R. 55 (1947) 331–333.
[35] K.R. Hall, L.C. Eagleton, A. Acrivos, T. Vermeulen, Ind. Eng. Chem. Fundam. 5 (1966) 212–223.
[36] S.J. Gregg, K.S.W. Sing, Adsorption, Surface Area and Porosity, Academic Press, London and New York, 1967, pp. 195–223.
[37] E.A. Bursali, L. Cavas, Y. Seki, S.S. Bozkurt, M. Yurdakoc, Chem. Eng. J. 150 (2009) 385–390.
[38] W. Rudzinsk, W. Plazinski, J. Phys. Chem. B 110 (2006) 16514–16525.
[39] Y.J. Wu, L.J. Zhang, C.L. Gao, J.Y. Ma, X.H. Ma, R.P. Han, J. Chem. Eng. Data 54 (2009) 3229–3234.
[40] T. Singh, R. Singhal, Desalin. Water Treat. (2013), http://dx.doi.org/10.1080/19443994.2013.808588.